

Biaxial shearing of star-shaped particles with multiellipse DEM model

Zhipeng Yu¹, Yang Li², and Haoran Jiang^{3,*}

¹Department of Engineering Mechanics and Energy, University of Tsukuba, Tsukuba, Ibaraki, 305-8573, Japan

²Department of Civil and Environmental Engineering, Northwestern University, Evanston, IL, 60208, USA

³Civil Engineering Design Division, Kajima Corporation, Minato-ku, Tokyo, 107-8477, Japan

Abstract. Using the multiellipse-based discrete element method (DEM), we numerically study the biaxial shearing behavior of granular materials composed of star-shaped particles. These particle shapes are generated by overlapping two or three identical ellipses with a common center of mass, while varying the aspect ratio from 1 to 5. Our results reveal that the macroscopic shear strength of the system increases monotonically with particle non-convexity. In contrast, the packing fraction exhibits a non-monotonic dependence on non-convexity, initially increasing and then decreasing as non-convexity further grows. This behavior reflects variations in the local pore size due to the competition between short-range ordering and excluded volume effects. Furthermore, microscopic analysis indicates that the increase in shear strength is linked to higher contact numbers and reduced contact and inter-grain distances, corresponding to stronger interlocking at higher non-convexity.

1 Introduction

The effects of particle shape on the behavior of granular materials across different regimes have been extensively studied. In particular, discrete element method (DEM), a well-established numerical tool, allows for the isolation and investigation of the influence of specific shape characteristics. Most research to date has focused on the impact of particle's overall form [1], local angularity [2], and surface roughness [3], collectively referred to as multiscale shape descriptors [4]. However, the role of particle non-convexity has received comparatively less attention, despite its prevalence in nature. While past studies [5] using disk-overlapping shapes show that non-convexity can significantly constrain particle's mobility and affect the stability of the granular aggregates, the involved numerical treatments in such shapes only lead to mild non-convexities. Only recently have researchers begun to investigate the unique behaviors of highly non-convex shapes, including the contact network of hexapods under static packing [6], the stress transmission of S-shaped hooks under quasi-static shearing [7], and the geometric cohesion of star-shaped particles observed during dynamic column collapse [8].

The aim of this study is to advance the understanding of the behavior of highly non-convex shapes by examining the micro-to-macro properties of granular systems composed of multiellipse-based shapes. This paper is organized as follows. Section 2 provides a brief description of the design of explored star-like shapes and numerical procedures used to evaluate the biaxial shearing responses of tested samples. Section 3 presents the simulation results, including the variations in stress ratio and packing fraction

during shearing, their critical-state averages as a function of the non-convexity index, and microscopic metrics for interlocking effects. Finally, Sec. 4 concludes with a summary of the key findings.

2 Methodology

2.1 Design of particle shape

We focus on the study of star-shaped, non-convex geometries modeled using clumps of ellipses. Specifically, two series of shapes are considered, generated by overlapping either 2 or 3 identical ellipses. In each series, the sub-ellipses share a common mass center but are rotated relative to each other by 60° or 90°, see Fig. 1. This configuration produces shapes with four or six arms, denoted as $N_a = 4$ and 6, respectively. The degree of non-convexity is modified by varying the aspect ratio (A_r) of the sub-ellipses within the range $A_r \in \{1, 1.2, 1.5, 2, 3, 5\}$, where $A_r = 1$ represents the circular shape. Altogether, we analyze a total of 11 granular systems, each characterized by a distinct level of non-convexity.

2.2 Multiellipse-based discrete element modeling for biaxial shearing tests

To model the interactions of star-shaped particles, we rely on an in-house DEM code that efficiently detects contacts between ellipses and implements the multiellipse clumping approach. Contact detection is based on an analytic expression for the distance of closest approach of the centers of two arbitrary ellipses [9]. Readers are referred to the original work for further details. For force calculations, we adopt a linear spring-dashpot contact model, with the tangential force capped by Coulomb's law of friction.

*e-mail: jiangh@kajima.com

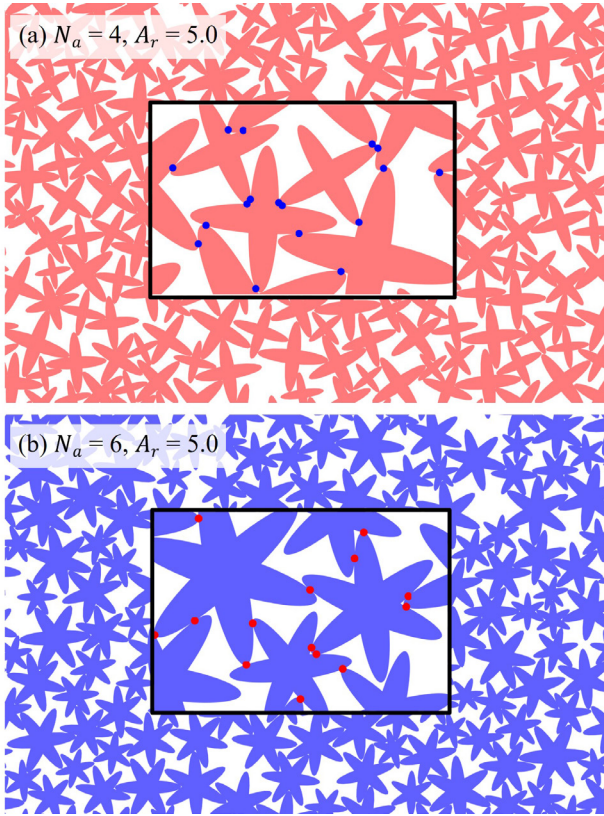


Figure 1. Close-up views of the numerical samples at the end of isotropic compression with zero friction between particles for (a) $N_a = 4, A_r = 5.0$ and (b) $N_a = 6, A_r = 5.0$.

The procedure for biaxial compression is as follows. Initially, specimens are generated by randomly placing 10,000 non-overlapping particles with the desired shapes in a bi-periodic domain. The diameters $\langle d \rangle$ of the circumscribed circles of these particles are uniformly distributed between 1mm and 2mm. In the following, $\langle d \rangle$ is used as the characteristic length. Mechanically stable packings are then prepared by isotropic compression, where the system stress reaches $\sigma_{xx} = \sigma_{yy} = 100\text{kPa}$. During this stage, the particles are set to be frictionless ($\mu_p = 0$) to achieve dense packings (see Fig. 1). Subsequently, μ_p is increased to 0.5 for the shearing phase. Biaxial loading is applied by decreasing the vertical boundary length at a constant rate while simultaneously adjusting the horizontal boundary length to enforce a constant stress of $\sigma_{xx} = 100\text{kPa}$. The loading rate $\dot{\epsilon}_1 = 0.1\text{s}^{-1}$ is kept low to satisfy the quasi-static condition. All samples are sheared up to a cumulative axial strain of $\epsilon_1 = 40\%$.

3 Results and discussions

3.1 Macroscopic stress–strain characteristics

On the macroscopic behavior of samples with different combinations of N_a and A_r , we show in Fig. 2 the variations in stress ratio q/p and volumetric strain ϵ_v (inset). For each N_a value, the typical stress peak characteristic of dense systems is observed, along with A_r -dependent constant stress values at the critical state. The critical state is

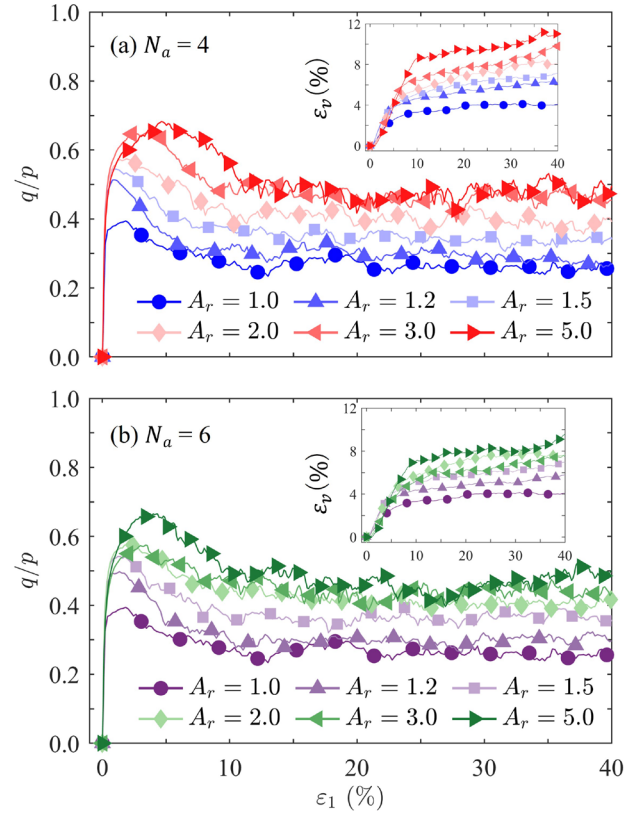


Figure 2. Stress ratio q/p and volumetric strain ϵ_v (insets) as a function of ϵ_1 for systems with (a) $N_a = 4$ and (b) $N_a = 6$.

defined as the range of $\epsilon_1 \in [20\%, 40\%]$, based on our observations of constant stress. Notably, both the peak and critical q/p values increase as the particles become more non-convex, accompanied by more pronounced volume expansion to accommodate particle rearrangements.

Figure 3 shows the shear strength at the critical state $\mu_c = (q/p)_c$ and the packing fraction ϕ (particle-to-domain volume ratio) at both initial and final states, plotted against the non-convexity index η . Here, η is defined as the void area to minimum circumscribed circle's area ratio for a shape (see Fig. 3a), increasing from 0 (circle) to 1 (infinitely large A_r) to indicate higher non-convexity. As anticipated, within each shape group, μ_c increases monotonically with η , although η does not collapse the data across the two series of shapes. The rate of increase in μ_c becomes more moderate at higher η , consistent with shear strength saturation observed in other non-circular shapes [1, 10]. In contrast, for both N_a values and at both the onset and end of loading, ϕ reaches a local maximum as η increases, then declines sharply with further increases in η . This non-monotonic variation reflects changes in local pore volume, driven by the competing effects of particle ordering and volume exclusion. The latter becomes increasingly dominant as the arms of the particles elongate. Compared to $N_a = 4$, systems with $N_a = 6$ exhibit stronger volume exclusion, as indicated by a less pronounced peak and an overall lower packing density. This occurs because a larger number of arms reduces the angle between two adjacent arms, thereby decreasing the probability that an arm

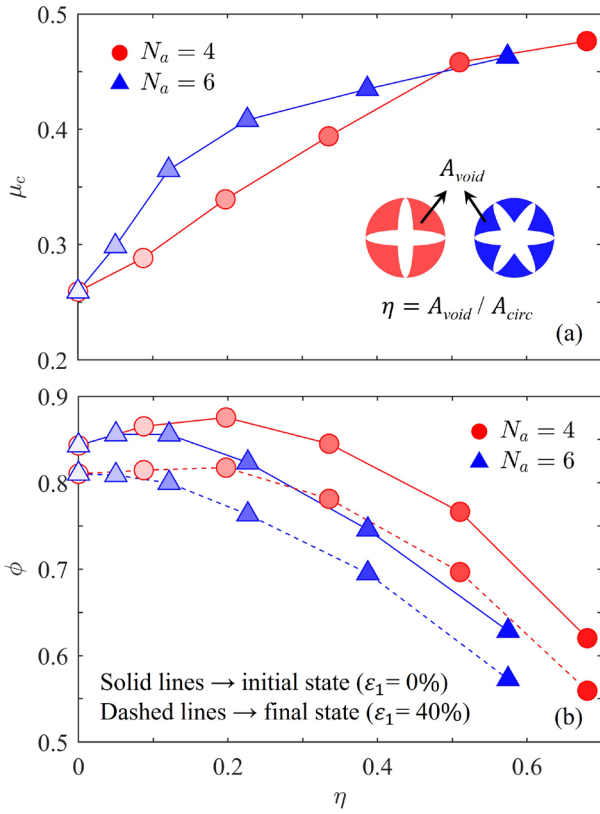


Figure 3. (a) Critical shear strength μ_c and (b) packing fraction ϕ at two strain levels as a function of non-convexity η .

of particle i will fit into the void created by two adjacent arms of particle j (Fig. 1).

3.2 Particle-scale analysis

The mean coordination number \bar{Z} , which represents the average number of contacts per non-floating particle, is key to understanding the internal structure of granular systems. Fig. 4 displays the evolution of \bar{Z} with respect to ε_1 , showing a rapid decline during the strain-hardening phase, followed by stabilization at shape-dependent values. We then show in Fig. 5 the initial and critical values of \bar{Z} as a function of η . It is noteworthy that, due to the non-convex nature of the particles, multiple contacts can occur between the same pair of particles and are counted separately. According to isostatic theory for perfectly rigid particles, two contacts per degree of freedom d_f are required to constrain a frictionless particle. This yields $Z = 4$ and $Z = 6$ for 2D circular and non-circular particles, respectively. The frictionless packings prepared in this study (solid lines) agree well with the theoretical predictions. As samples are loaded into the critical state, \bar{Z} decreases in all cases due to volume expansion, primarily resulting from the loss of contacts in the horizontal direction. Nevertheless, particles with higher η tend to exhibit a larger proportion of multiple-contact mode and retain a relatively higher number of contacts (dashed lines), as their arms more readily interlock. Moreover, for the same level of η , samples with $N_a = 6$ exhibit slightly larger \bar{Z}_c values, which may

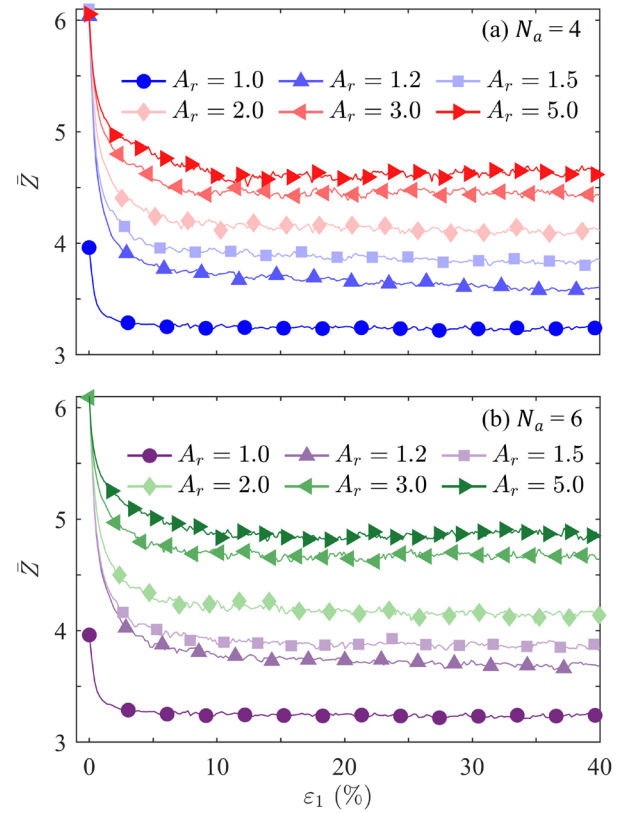


Figure 4. Mean coordination number \bar{Z} as a function of ε_1 for systems with (a) $N_a = 4$ and (b) $N_a = 6$.

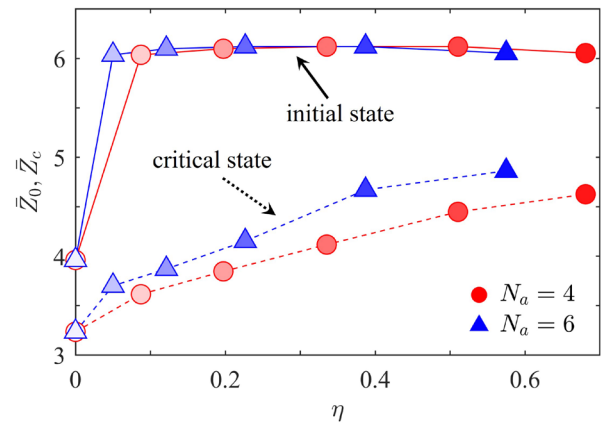


Figure 5. Mean coordination number in the initial state (\bar{Z}_0) and in the critical state (\bar{Z}_c) as a function of non-convexity η .

partially explain the observed variations in μ_c of these two shape species shown in Fig. 3a.

Our next focus is on the evaluation of interlocking effects, where particles surrounded by more neighbors are more likely to restrict each other's mobility. To quantify this feature, we first present the distribution of the inter-center distance l between two contacting particles in Fig. 6. Note that we focus on the critical state, and the distance is normalized by $\langle d \rangle$. For two values of N_a , the $l/\langle d \rangle$ distribution is broader at higher A_r , with a minimum distance occurring when particles align their arms

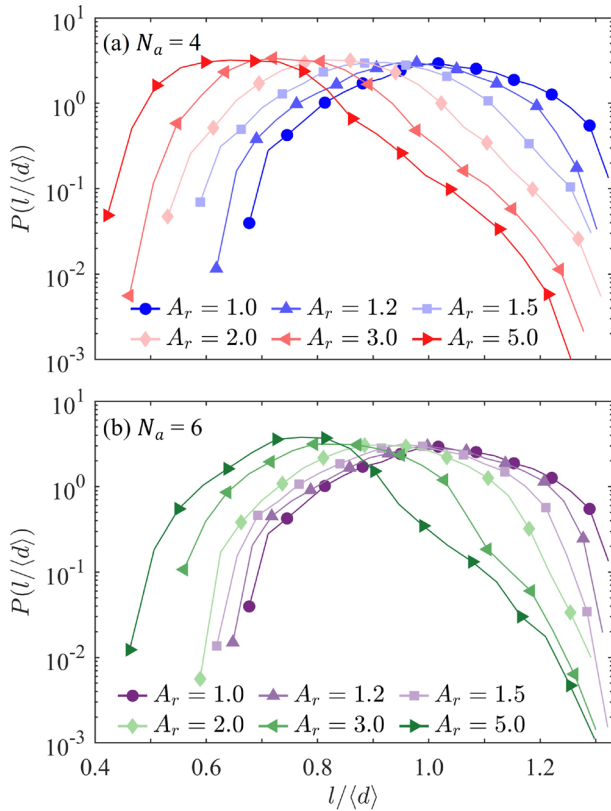


Figure 6. PDFs of normalized branch vector lengths $l/\langle d \rangle$ for systems with (a) $N_a = 4$ and (b) $N_a = 6$ in the critical state.

in an ordered manner. For circular systems, a distribution is also observed due to the size dispersity employed in our study. Next, we evaluate the radial distribution function $g(r)$, which quantifies the normalized number of particle centers within a circle of radius r centered on a given particle. The results, shown in Fig. 7, describe the spatial arrangement of particles surrounding a reference particle. The data indicate a distinct shift of the peaks to shorter distances as A_r increases, suggesting that, despite the excluded-volume effects, non-convex shapes can still position closely together due to their unique geometries. In contrast, for circular particles, the peaks in $g(r/\langle d \rangle)$ occur at positive integers (1, 2, ...), reflecting their simpler geometry. Overall, these observations provide clear evidence of locally strong interlocking in non-convex shapes.

4 Conclusions

In this study, we conduct a series of DEM simulations using star-shaped particles modeled as multiellipse clumps to examine the effects of non-convexity on shearing behaviors. Macroscopically, we identify a non-monotonic relationship between packing fraction and particle non-convexity, which can be attributed to the enhanced volume exclusion effects. In contrast, the shear strength of the system increases monotonically with non-convexity. This indicates that while longer particle arms lead to looser packings, they also significantly enhance the interlocking effects to increase the stability. Microscopic anal-

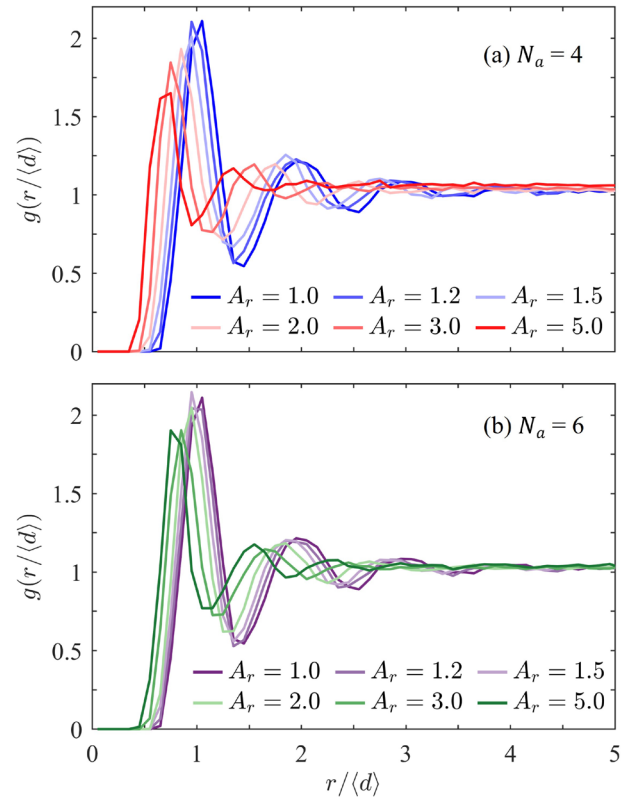


Figure 7. Radial distribution function $g(r/\langle d \rangle)$ for systems with (a) $N_a = 4$ and (b) $N_a = 6$ in the critical state.

ysis supports this observation, showing that higher non-convexity leads to more contacts and shorter contact and inter-particle distances. While both shape series show similar trends with increasing non-convexity, the chosen shape index fails to provide a unified description, highlighting the need for a more comprehensive descriptor.

References

- [1] H. Jiang, R. Kawamoto, Y. Li, *Computers and Geotechnics* **169**, 106235 (2024)
- [2] T. Binaree, E. Azéma, N. Estrada, M. Renouf, I. Preechawattipong, *Physical Review E* **102**, 022901 (2020)
- [3] H. Jiang, O.C. Debanath, F. Chen, R. Kawamoto, Y. Li, *Powder Technology* **445**, 120078 (2024)
- [4] J. Zheng, R.D. Hryciw, *Géotechnique* **65**, 494 (2015)
- [5] Z. Nie, S. Liu, W. Hu, J. Gong, *Particology* **52**, 105 (2020)
- [6] T.D. Tran, S. Nezamabadi, J.P. Bayle, L. Amarsid, F. Radjai, *Soft Matter* **20**, 3411 (2024)
- [7] K. Karapiperis, S. Monfared, R.B.d. Macedo, S. Richardson, J.E. Andrade, *Granular Matter* **24**, 91 (2022)
- [8] D. Aponte, N. Estrada, J. Barés, M. Renouf, E. Azéma, *Physical Review E* **109**, 044908 (2024)
- [9] X. Zheng, P. Palffy-Muhoray, *Physical Review E* **75**, 061709 (2007)
- [10] H. Jiang, R. Kawamoto, T. Matsushima, *Journal of Structural Engineering, A* **70**, 141 (2024)